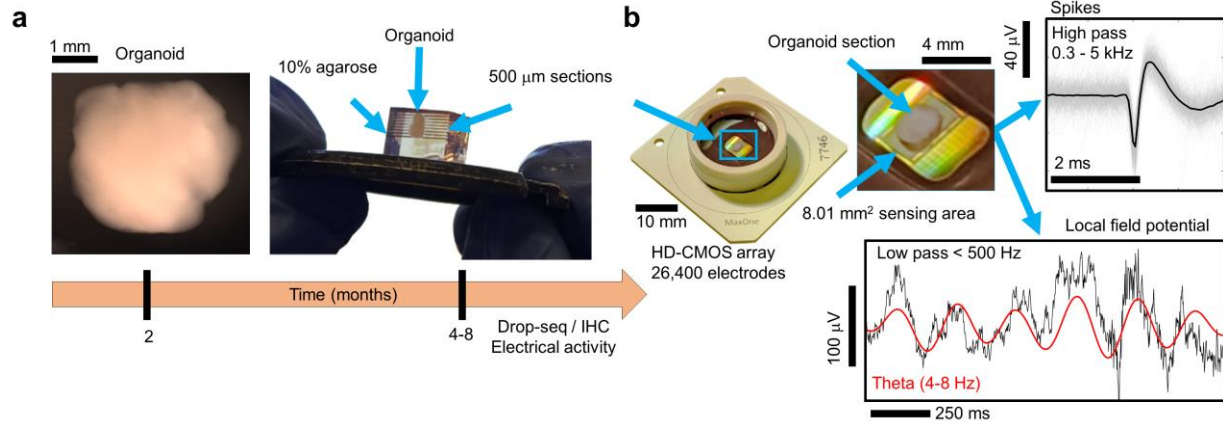


Supplementary Information for
**Functional neuronal circuitry and oscillatory dynamics in human
brain organoids**

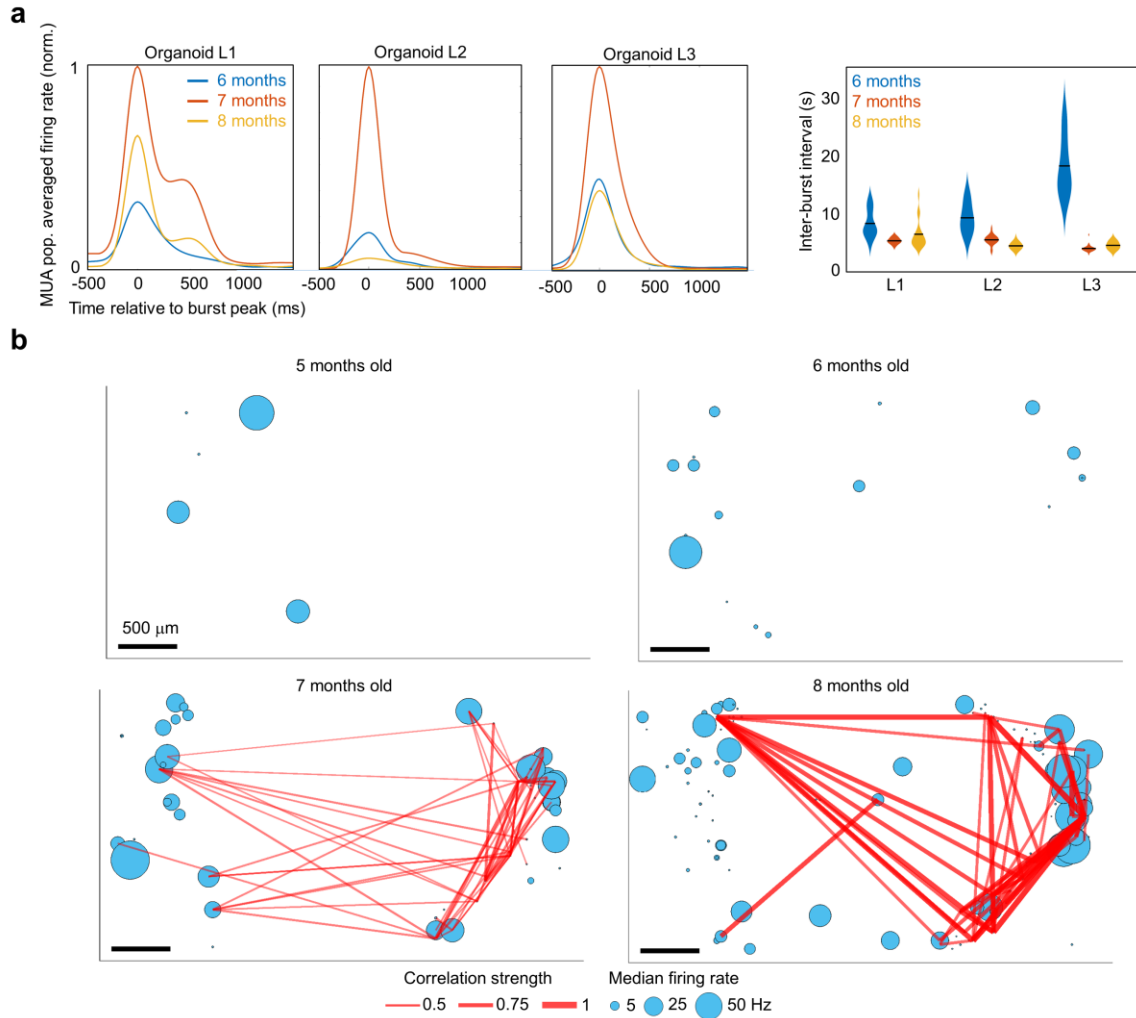
Tal Sharf, Tjitse van der Molen, Stella M.K. Glasauer, Elmer Guzman, Alessio P. Buccino, Gabriel Luna, Zhuowei Cheng, Morgane Audouard, Kamalini G. Ranasinghe, Kiwamu Kudo, Srikantan S. Nagarajan, Kenneth R. Tovar, Linda R. Petzold, Andreas Hierlemann, Paul K. Hansma, Kenneth S. Kosik

This PDF file includes:

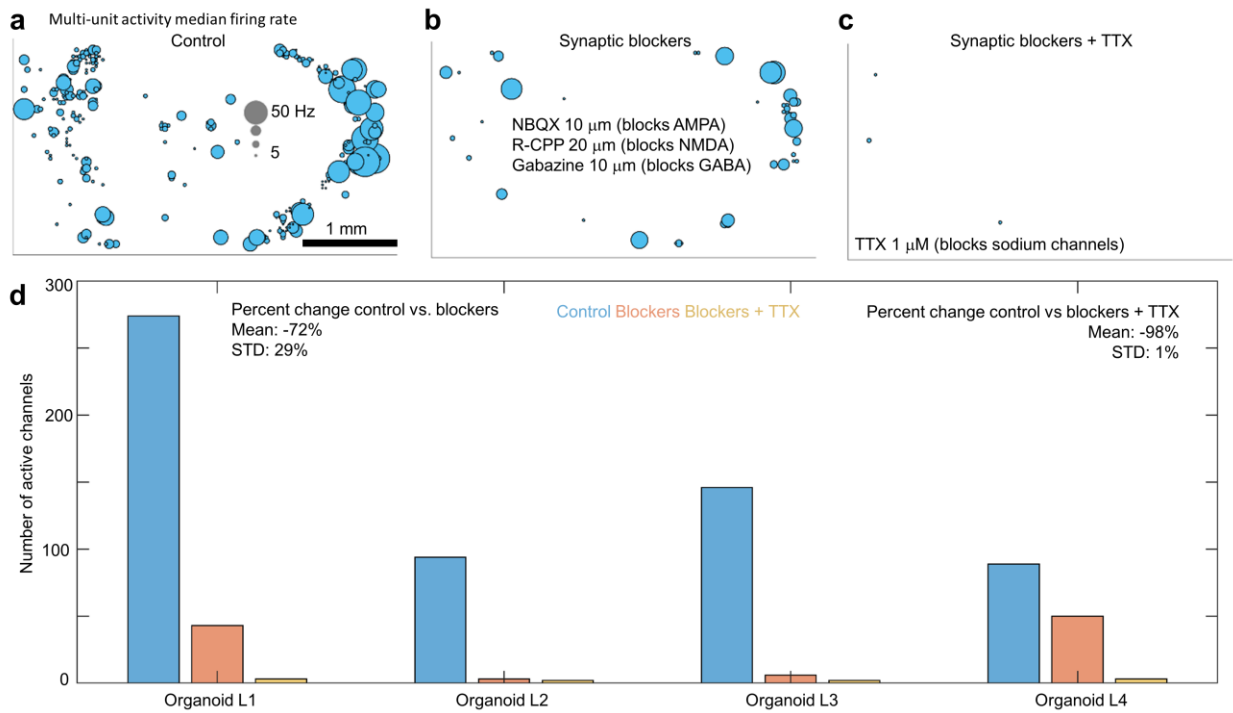
Supplementary Figures 1 to 21
Supplementary Legends 1 to 3



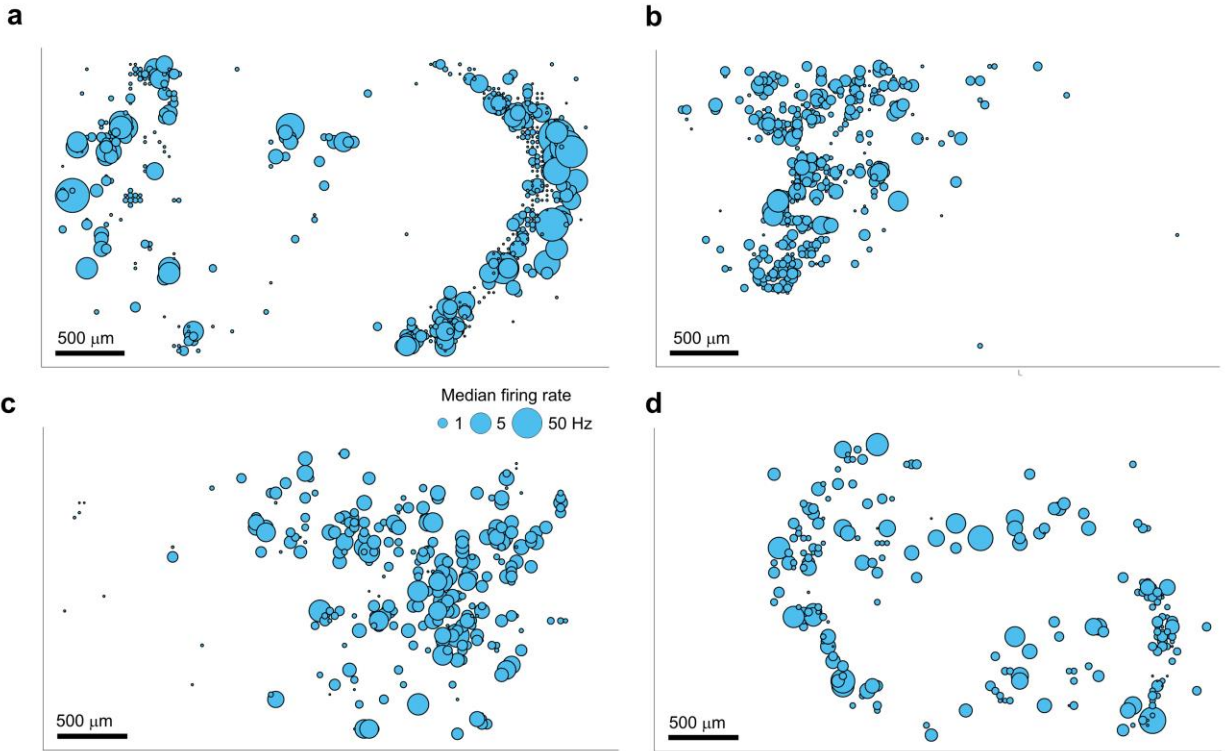
Supplementary Fig. 1. Human brain organoid preparation for electrophysiology. **a** Left, picture of a brain organoid at 2 months, scale bar is 1 mm. Right, organoids (4-6 months old) were imbedded in 10% agarose and sectioned into 500 μm thick slices. **b** Organoid slices were then placed on high-density CMOS microelectrode arrays (26,400 recording electrodes spanning across surface area of $\approx 8.01 \text{ mm}^2$ with a center-to-center distance of 17.5 μm). High bandwidth recordings reveal the presence of high frequency ($\approx 1 \text{ ms}$) extra-cellular action potentials (spikes) as well as low-frequency components of the local field potential in the theta range (4-8 Hz), see Methods and Supplementary Fig. 2 for characterization of electrical activity.



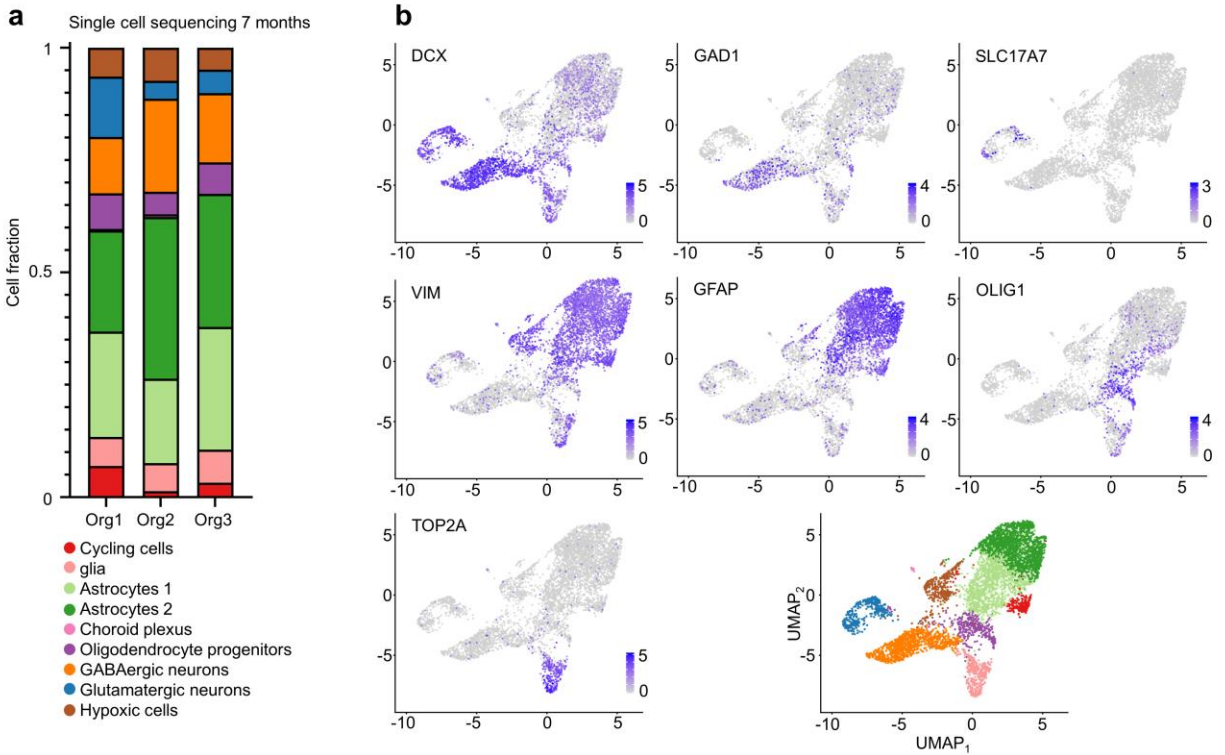
Supplementary Fig. 2. Overview of organoid spiking activity at different time points on arrays. **a** Left, the multi-unit activity (MUA) population-averaged firing rate (pop. rate) is shown at different developmental time points for $n = 3$ organoids and shows a peak in activity at 7 months. Right, the inter-burst intervals are shown. The number of inter-burst intervals at 6, 7 and 8 months are 3,12,5; 20,20,27; 12,25,24 for organoid L1, L2 and L3 respectively. **b** Median firing rate from single-unit activity (blue circles) and pairwise spike correlation strengths (red lines) are shown for organoid L1 at different developmental time points (5, 6, 7, 8 months old).



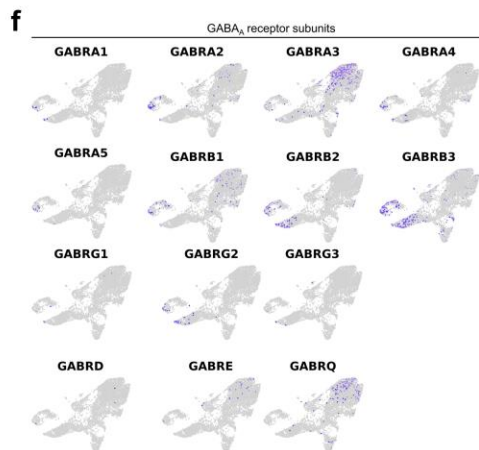
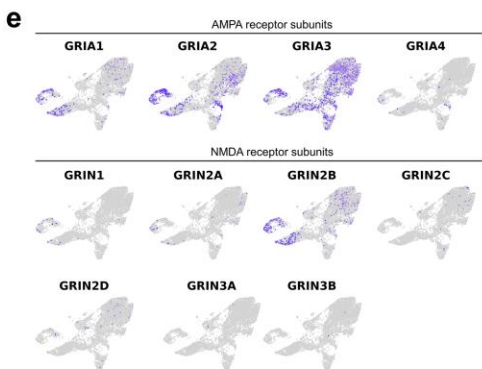
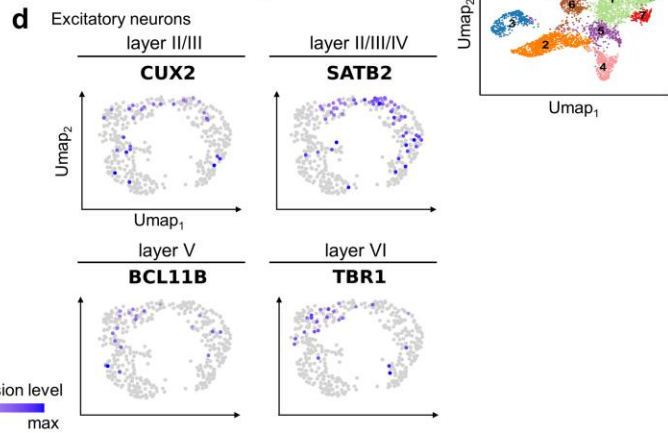
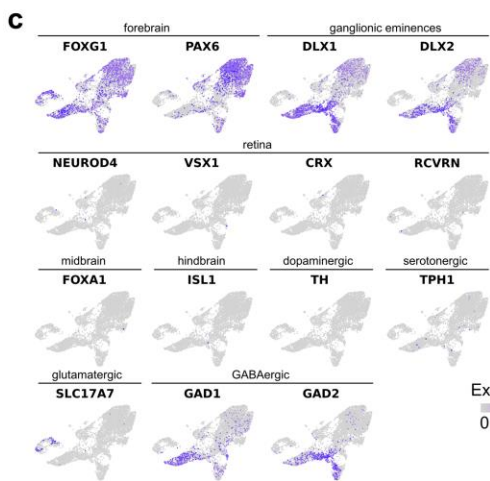
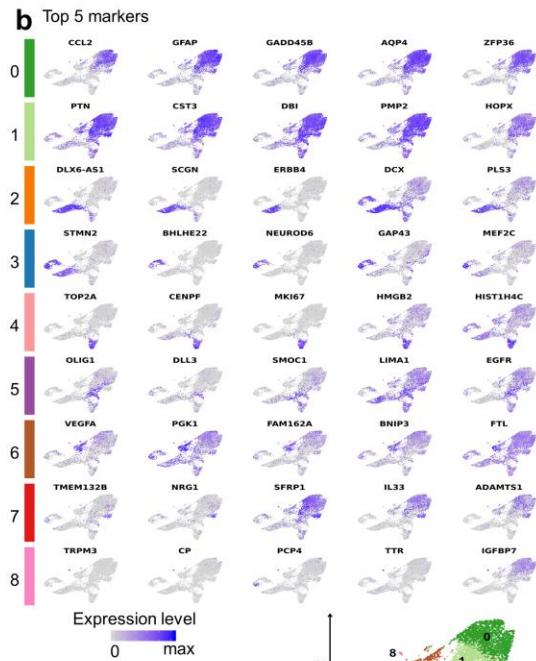
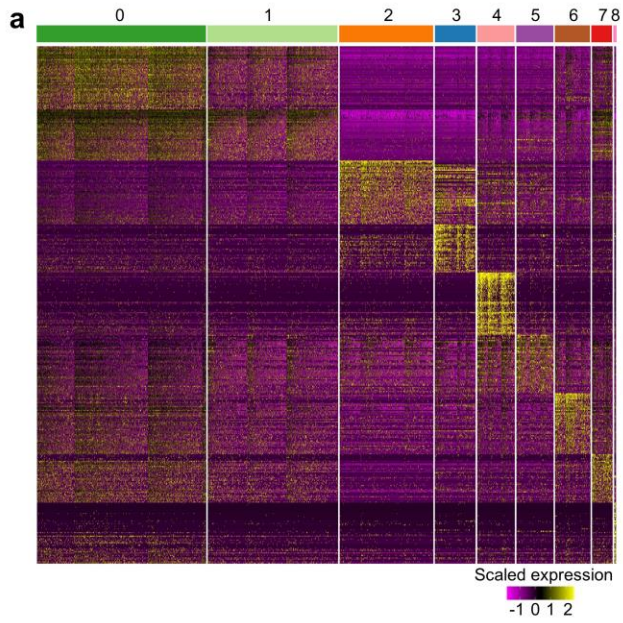
Supplementary Fig. 3. Synaptic and sodium channel blockers. **a-c** The median firing rate calculated from multi-unit spiking activity is shown. The addition of synaptic blockers reduced spiking activity by $72\% \pm 29\%$ (mean \pm STD) at saturating concentrations 10 μM NBQX (blocks AMPA), 20 μM R-CPP (blocks NMDA) and 20 μM gabazine (blocks GABA_A). The addition of 1 μM tetrodotoxin (TTX) reduced detected spikes by $98\% \pm 1\%$ (mean \pm STD) across $n = 4$ organoids. The remaining small number spike events can be attributed to false detected spikes due to electronic noise. **d** The number of active electrode (with at least 30 spikes) are shown across $n = 4$ organoids for the same conditions shown in **a-c**.



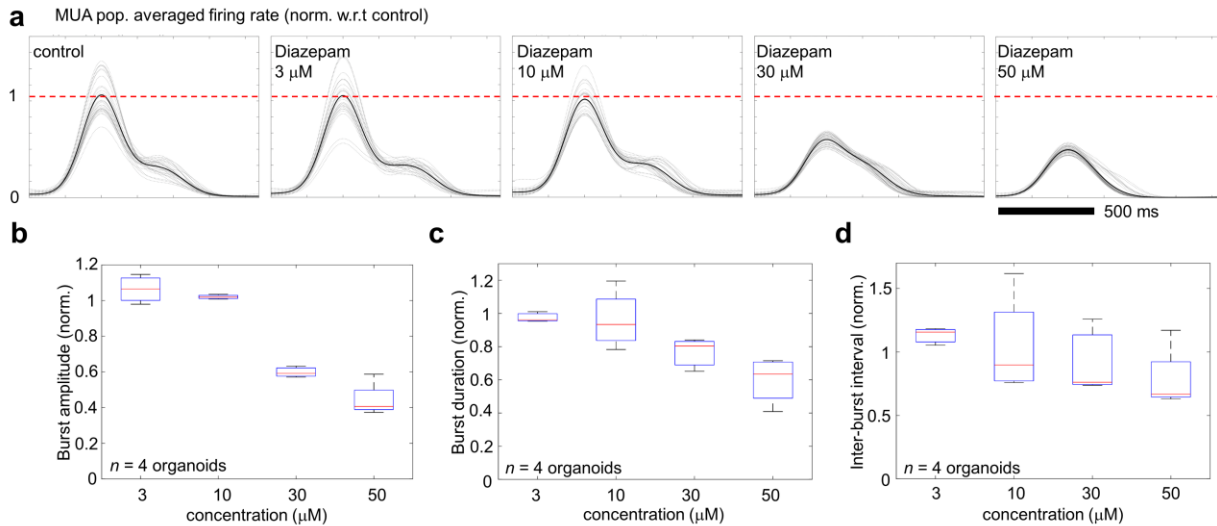
Supplementary Fig. 4. Overview of spatial spiking patterns across organoids. The median firing rate measured by individual electrodes (multi-unit activity) are shown across the organoid. **a** Organoid L1 at 7 months old. **b, c** Organoid L2 and L3 at 8 months, respectively. **d** Organoid L5 at 6 months old.



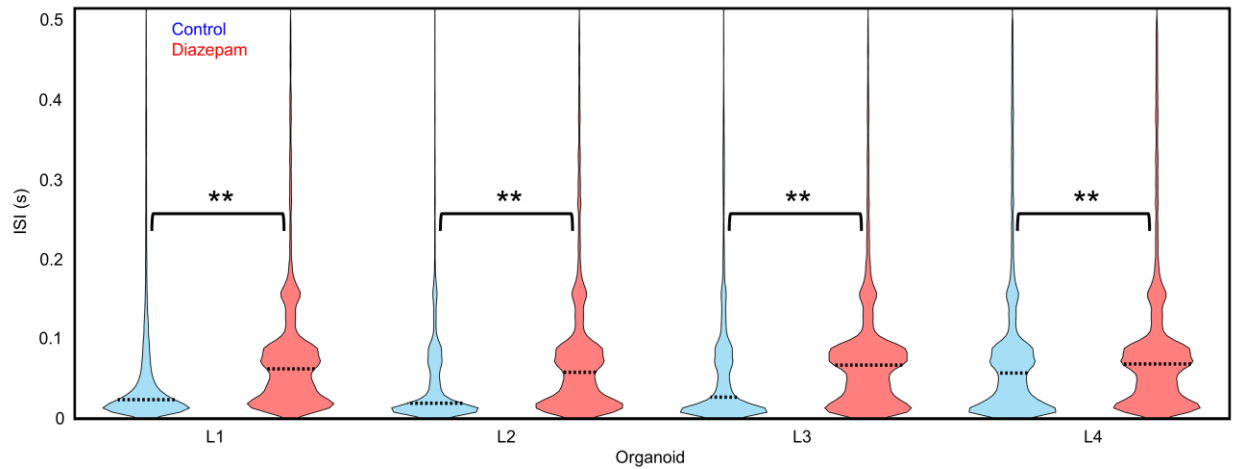
Supplementary Fig. 5. Human brain organoid identification of cell types using single-cell sequencing. **a** Relative proportions (fractions) of cell types identified in the 3 individually sequenced 7-month-old organoids as determined by drop-seq. **b** Selection of canonical markers used to identify cell types in single-cell data. UMAP plots are colored by normalized and scaled expression values. DCX: neurons; GAD1: GABAergic neurons; SLC17A7: glutamatergic neurons; VIM: glia; GFAP: astrocytes; OLIG1: oligodendrocyte progenitors; TOP2A: cycling cells. Bottom right UMAP plot is colored by cluster.



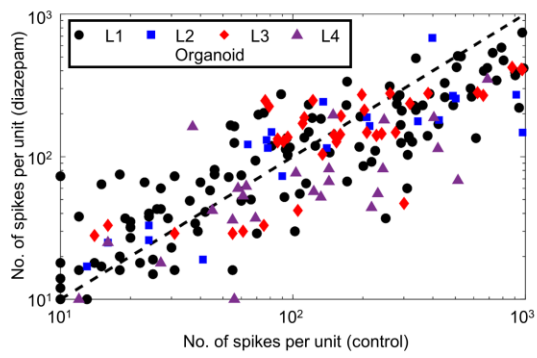
Supplementary Fig. 6. Cellular identities and neurotransmitter profiles of brain organoids determined by single-cell transcriptomics. **a** Heatmap of the top 50 marker genes for each cluster, colored by z-scaled expression values. **b** Expression patterns of top 5 marker genes for each cluster. UMAP plots show expression levels (normalized and scaled) of the top 5 marker genes for each cluster. **c** Expression patterns of brain-region specific marker genes reveal predominant forebrain identity of the brain organoids used in this study. **d** Expression of pyramidal layer markers in glutamatergic neurons. Glutamatergic neurons were extracted from the dataset and projected as UMAP. Plots are colored by expression of selected cortical layer markers. **e** Organoids express multiple genes encoding subunits of AMPA- and NMDA-types of glutamate receptors. UMAP plots are colored by expression level of all known genes encoding subunits of AMPA and NMDA receptors. **f** Organoids express multiple genes encoding GABA_A receptor subunits. UMAP plots are colored by all known and detected genes encoding GABA_A receptor subunits. Not detected in single-cell data were GABRA6 and GABRP.



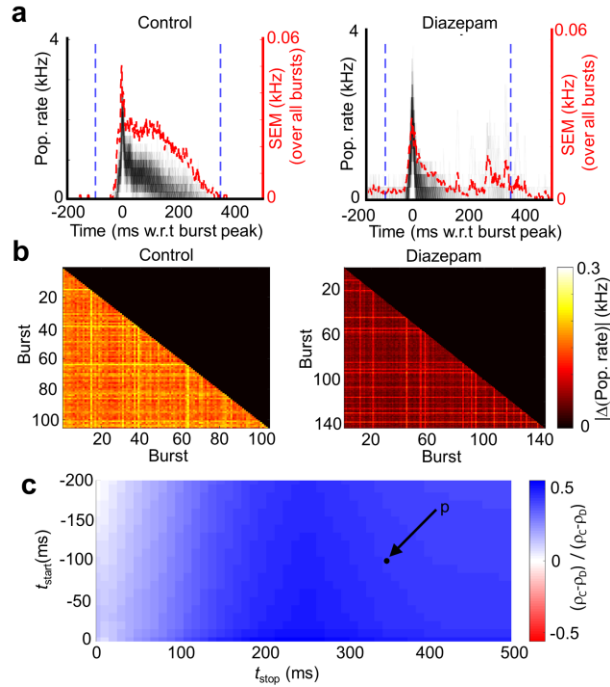
Supplementary Fig. 7. Pharmacological effects on spiking activity. **a** Multi-unit activity (MUA) population averaged firing rate (20 ms average sliding window smoothed with a 100 ms Gaussian kernel) for organoid L1 at 7.7 months old for control (left) and increasing concentrations of diazepam (3, 10, 30, 50 μ M) measured over 120 s. The gray lines are MUA population rates plotted for each burst (relative to the burst peak), the black line is the average across all bursts. **b-d** Mean burst amplitudes, burst durations and inter-burst intervals are reduced for diazepam concentrations greater than 10 μ M for *n* = 4 organoids. Values are normalized with respect to control conditions. The center red line indicates the median, the bottom and top edges of the box indicate the 25th and 75th percentiles, respectively. The whiskers extend to the minimum and maximum data points.



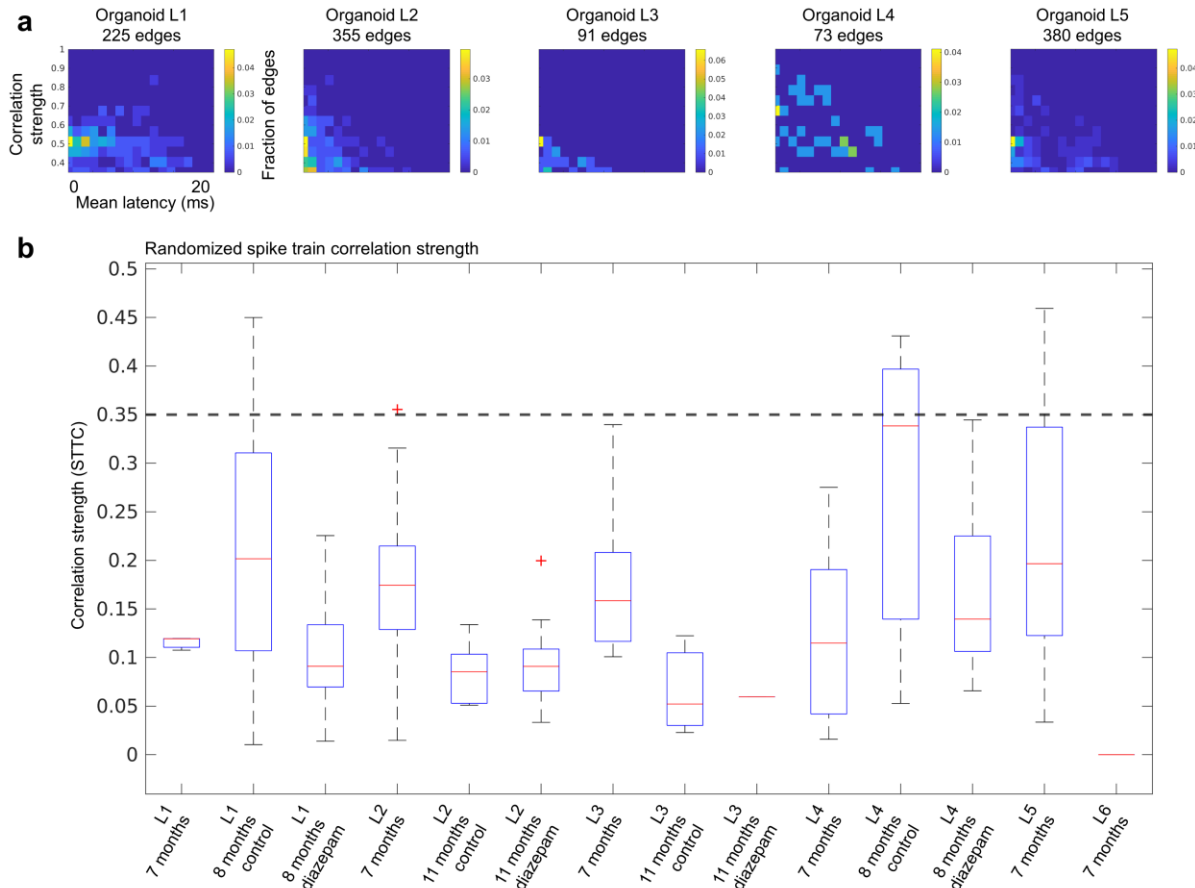
Supplementary Fig. 8. Interspike interval shifts. A pronounced shift towards larger ISI distributions is clearly observed with diazepam (50 μ M) when plotting the distribution of ISIs across all units (shown by the violin plots) for four organoids as determined by a two-sample KS test ($P < 1 \text{ e-}4$, $P < 1 \text{ e-}4$, $P < 1 \text{ e-}4$, $P < 1 \text{ e-}4$ for organoids L1, L2, L3 and L4) relative to control.



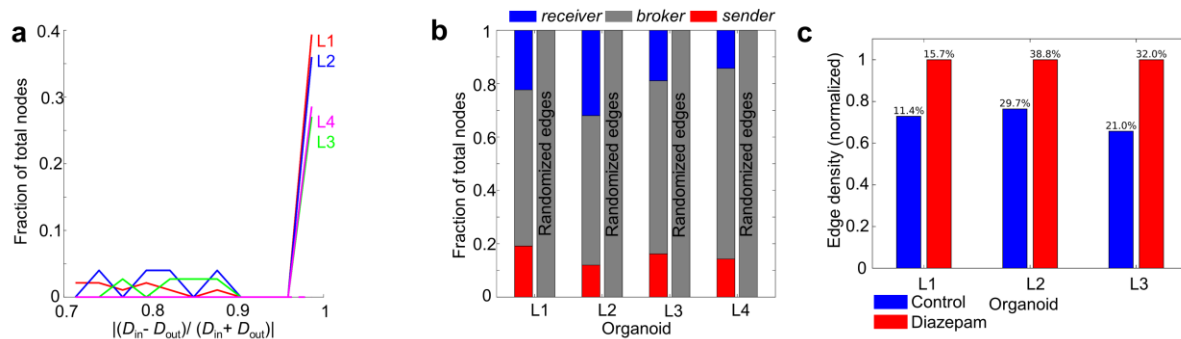
Supplementary Fig. 9. Total number of single-unit spikes under control conditions plotted against the number of single-unit spikes under diazepam (50 μ M) conditions remain similar across $n = 4$ organoids.



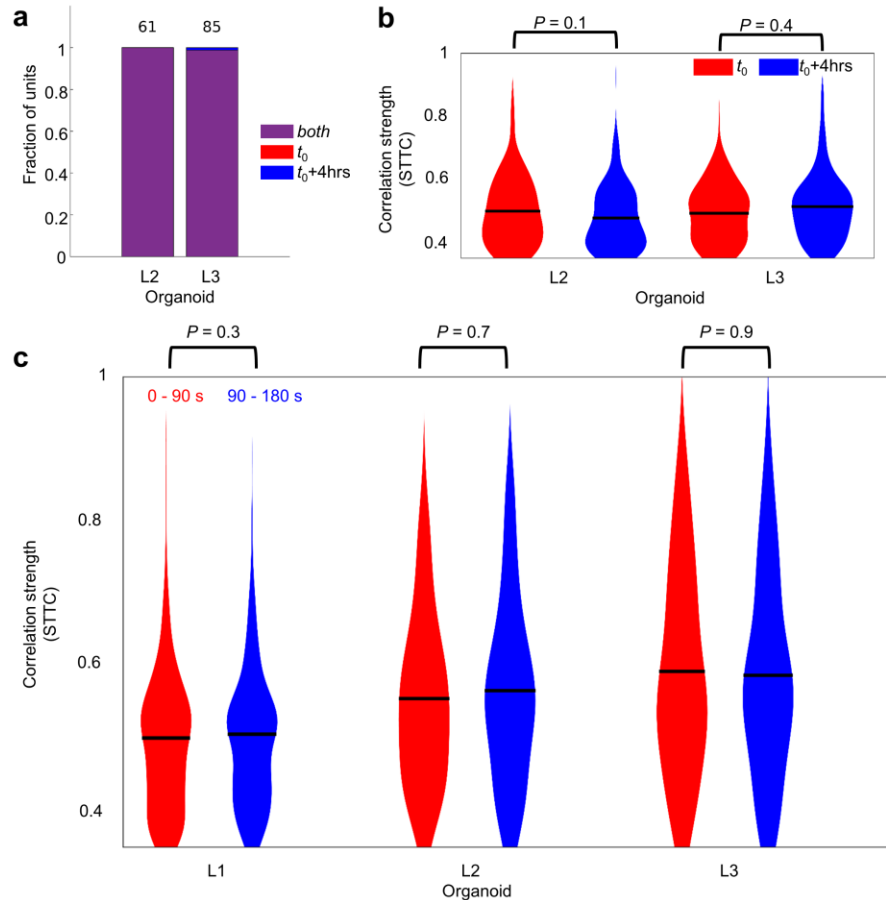
Supplementary Fig. 10. Variation in population-level dynamics for organoid L2. **a** The population averaged firing rate for the control and diazepam recordings calculated from single-unit activity averaged over a 5 ms window. The population rate for each burst is plotted individually, centered by the peak in multi-unit activity (MUA). The standard error of the mean (SEM) calculated over all bursts is plotted in red. **b** The average difference in the population rate is shown across all individual burst pairs for the control and diazepam (50 μM) recordings from the same organoid. The average population rate difference is computed over a time window of -100ms until +350ms relative to the MUA peak (blue dotted line in **a**). The color bar scale is the same for control and diazepam. **c** Fractional change between population rate for control and diazepam $(\rho_C - \rho_D) / (\rho_C + \rho_D)$, averaged over a range of different time windows for L2. Here, ρ_C and ρ_D are the average difference in the population rate (for a given time interval t_{start} and t_{stop}) for control and diazepam, respectively. Blue tiles indicate a higher average population vector difference for control. The black dot ($P = (-100, 350)$ ms) indicates the time window used in **b**.



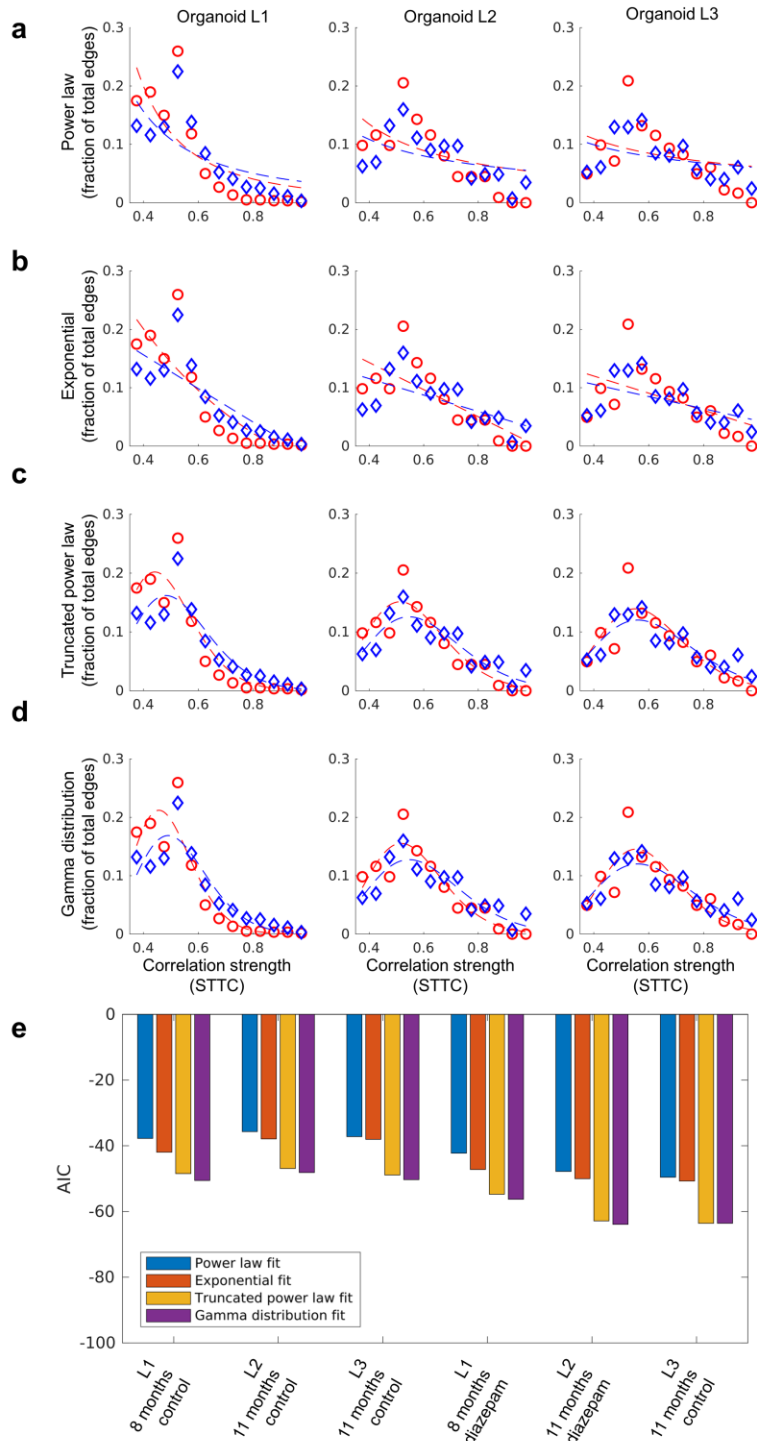
Supplementary Fig. 11. Latency distributions. **a** Pair-wise spike latency distributions as a function of correlation strength for $n = 5$ organoids at 7 months old consisting of unimodal latency distributions with a FWHM < 15 ms. Multimodal latency distributions (Hartigan's dip test $P < 0.1$) were excluded. Organoid L6 is not plotted due to low number of edges. **b** Connectivity edge strength distributions for randomized spike data from six organoids are shown for multiple measurements (see Methods); $93.2\% \pm 14.7\%$ of the connectivity edges strengths were below the 0.35 threshold ($n = 6$; 13 separate measurements). Organoid L3 at 11 months for diazepam treatment only had one edge while L6 had no pairwise spike correlations (edges) after spike train randomization and was excluded from the statistics above. The center red line indicates the median, and the bottom and top edges of the box indicate the 25th and 75th percentiles, respectively. The whiskers extend to the most extreme data points not considered outliers, and the outliers are plotted individually using the '+' marker symbol.



Supplementary Fig. 12. Pairwise spike correlation node and edge distributions. **a** The fraction of total nodes is plotted as a function of the absolute value of the fractional difference in node degree $|(D_{in} - D_{out}) / (D_{in} + D_{out})|$, where D_{in} and D_{out} are the number of incoming and outgoing edges, respectively, as determined by the pairwise correlation between single-units (nodes). The distributions are shown for four organoids. **b** Bar plots indicate that the relative fraction of ‘sender’, ‘brokers’ and ‘receivers’ nodes remain similar across four organoids. Nodes for which at least 90% of the edges are outgoing or incoming (which results in the 0.8 cutoff value), are chosen as senders/receivers. Randomizing the pairwise correlation network by performing degree preserving double edge swaps yielded no sender or receiver nodes. **c** The edge density between the largest component of interconnected nodes increases for diazepam (50 μ M) relative to control. For visual clarity the plots are normalized relative to control conditions. The edge density percentile of the observed network is shown above the bar plots.

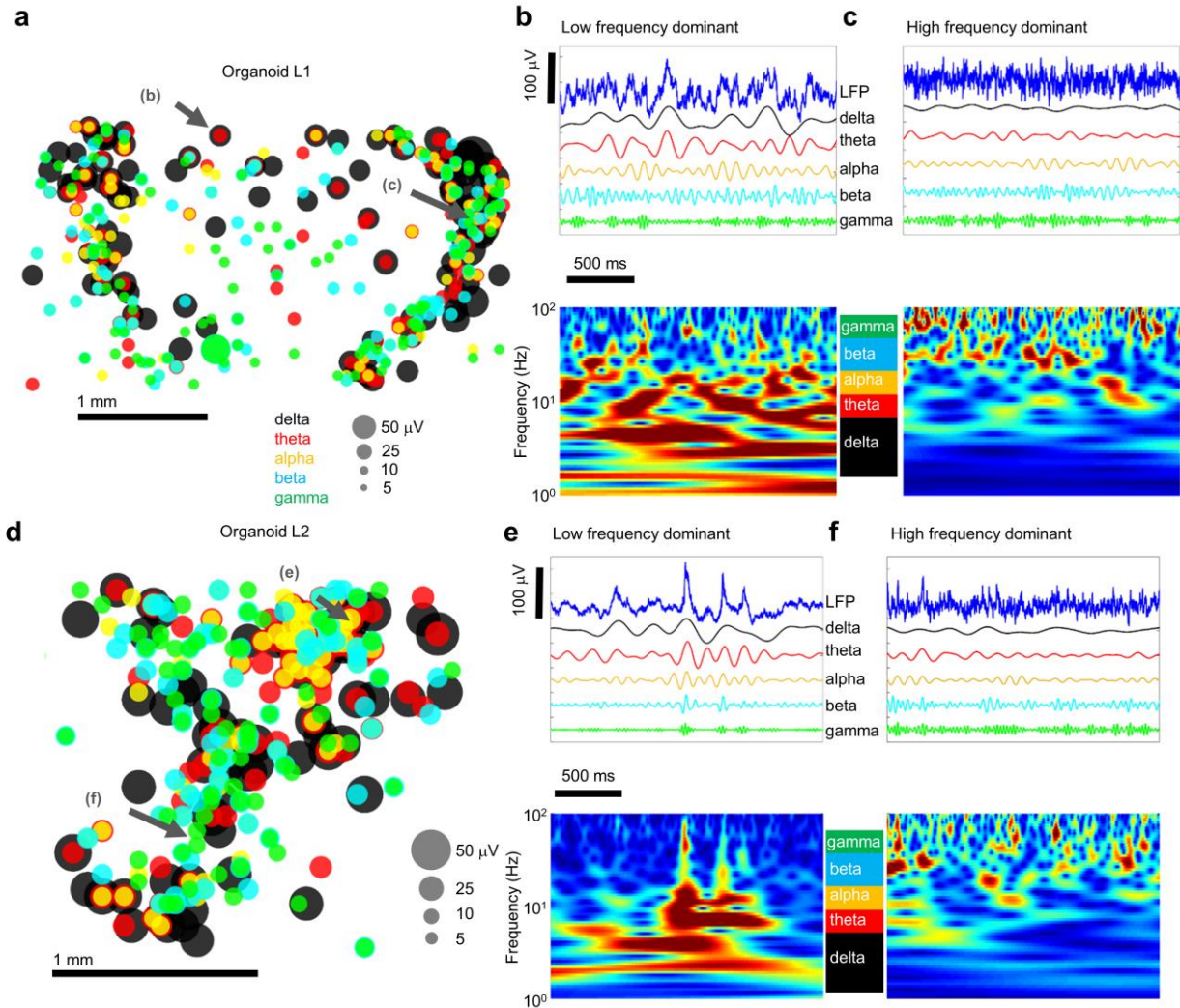


Supplementary Fig. 13. Stability of active units. **a** The number of active spiking units remain similar for two separate recordings taken at time t_0 and $t_0 + 4$ hours for two organoids (8-months old). Purple bars indicate the number of units active for both recordings, the red and blue bars represent the number of unique units at time t_0 and $t_0 + 4$ hrs, respectively. **b** The distribution of edge strengths determined from the spike time tiling coefficient (STTC) are not significantly different as determined by two-sample KS test ($P \geq 0.1$) when comparing the initial recording at time t_0 (red) and time $t_0 + 4$ hours (blue) for the same two organoids. The number of edges for time point t_0 are 85 and $t_0 + 4$ hrs are 154 for organoid L2 and 120 and 212 for organoid L3, respectively. **c** The distribution or pairwise edge strengths did not vary significantly over minute long timescales as determined by a two-sample KS test ($P \geq 0.3$). Three-minute-long recordings were split into 90 second blocks, the first 90 seconds of data are shown in red and the second 90 seconds are shown by the blue distributions.

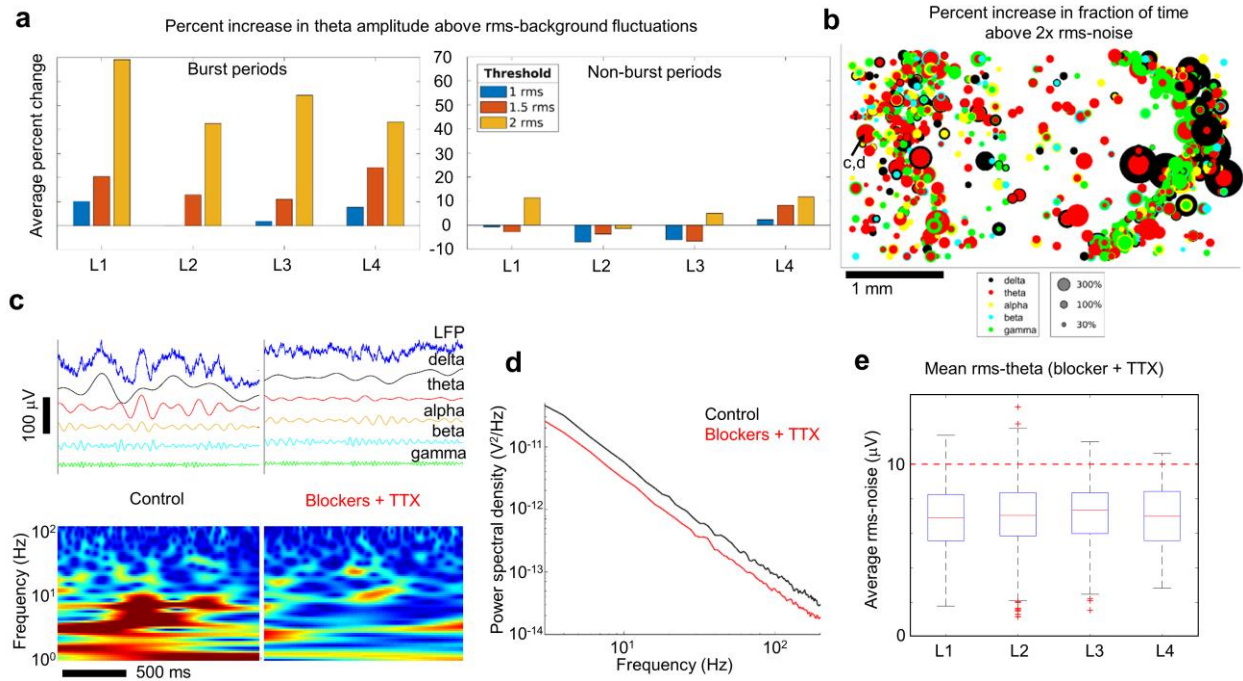


Supplementary Fig. 14. Edge strength scaling relationships details for control and diazepam data. **a** Power law ($y = a \cdot x^b$). **b** exponential ($y = a \cdot e^{-cx} + d$). **c** truncated power law ($y = a \cdot x^b \cdot e^{-cx}$). **d** Gamma distribution ($y = (a / (\Gamma(b) \cdot c^b)) \cdot x^{b-1} \cdot e^{-x/c}$). Fits to the edge strength distributions (edge strengths determined by the spike time tile coefficient (STTC)) were performed on the largest components of the functional connectivity networks. **e** Akaike information criterion (AIC) (see Diazepam comparison section of Methods for details) of the

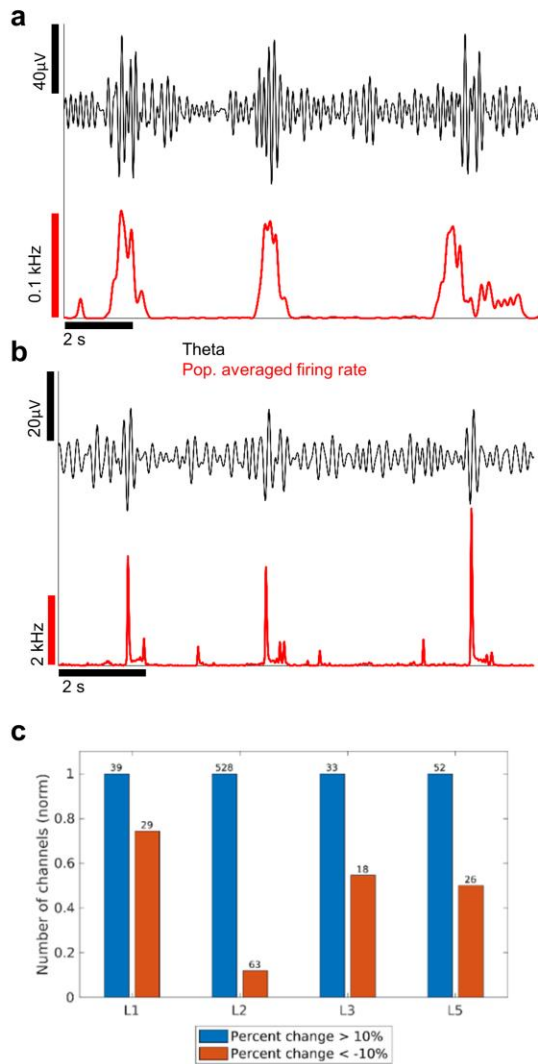
fitted data indicates that the gamma distribution results are the best fit of the edge strength distributions for $n = 3$ organoids.



Supplementary Fig. 15. Overview of LFP bands: spatial amplitudes, sub-band filtering and spectrograms. **a** Amplitude map of local field potential (LFP) sub-bands, the top ten percent per band are shown by amplitude: delta (0.5-4 Hz), theta (4-8 Hz), alpha (8-13), beta (13-30) and gamma (30-50 Hz). **b** Top, electrode site with dominant low frequency component of the LFP. Bottom, spectrogram of the LFP is shown. **c** Same as **b** for an electrode with a dominant high frequency component of the LFP. Organoid L1 at 8 months old. **d-f** Same as previous panels for organoid L2 at 8 months old.

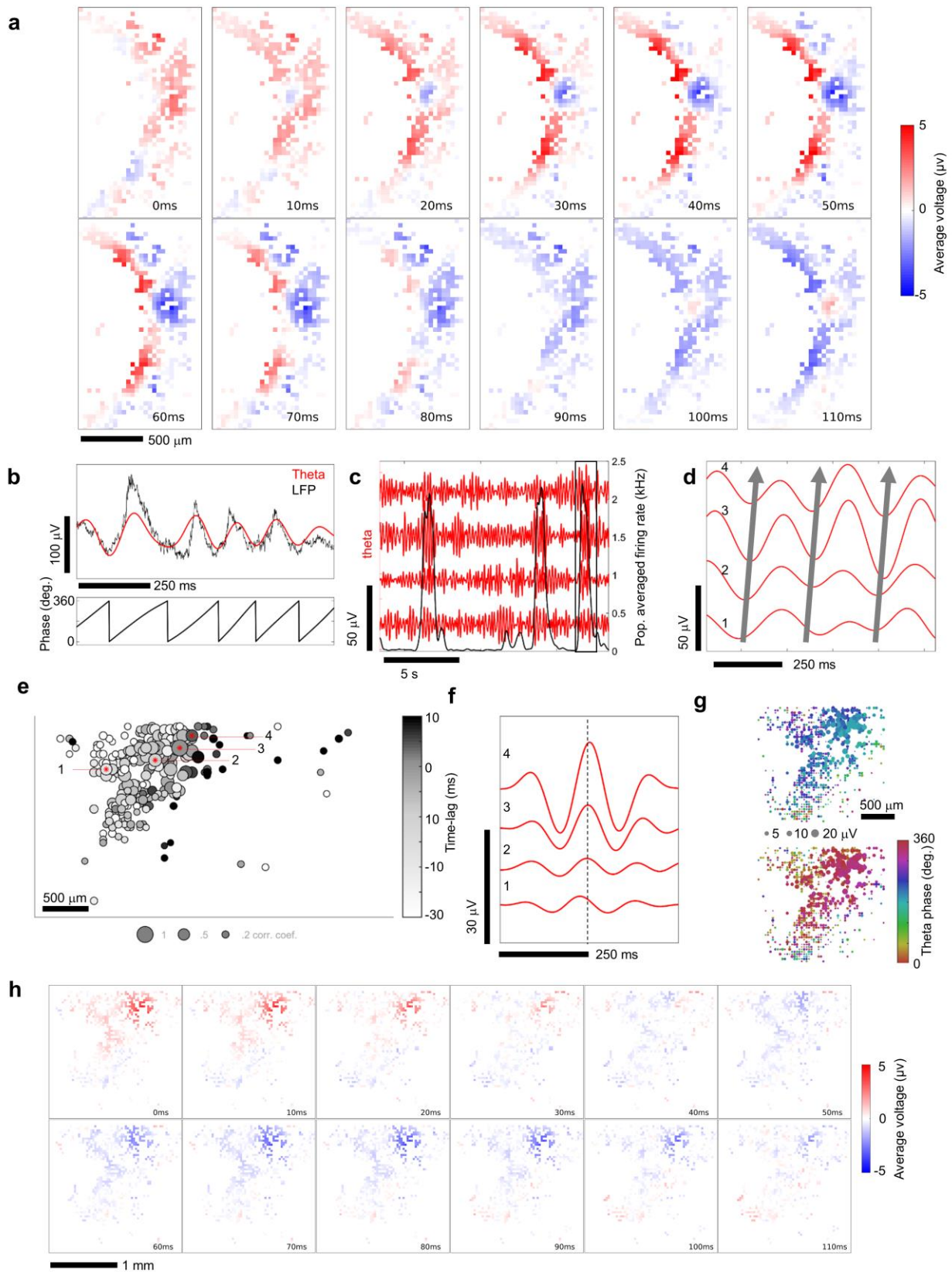


Supplementary Fig. 16. Synaptic blockers and TTX attenuate LFP amplitude. **a** Left, theta oscillation amplitude spent more time above the noise floor during population bursts compared to the amplitude measured with synaptic blockers + TTX. Right, there is no observable difference between theta amplitude time spent above the noise floor during non-burst periods compared to blockers + TTX ($n = 4$ organoids). **b** The fraction of time that the signal amplitude falls above 2 times the noise rms for burst periods compared to blockers + TTX recordings shows increased amplitudes in all frequency bands, dispersed over the whole array (organoid L1 at 8 months). **c** Example of the raw and decomposed signal of the channel specified in **b** during the control recording and the recording of the organoid treated with blockers and TTX. **d** The power spectral density is shown for the LFP of the channel specified in **b** shows a decrease in spectral power for all frequencies after treatment with blockers and TTX. **e** The empirical theta LFP noise floor threshold of $10 \mu\text{V}$ lies roughly 1.5 STD above the rms theta band noise levels measured across $n = 4$ organoids treated with blockers and TTX. The center red line indicates the median, and the bottom and top edges of the box indicate the 25th and 75th percentiles, respectively. The whiskers extend to the most extreme data points not considered outliers, and the outliers are plotted individually using the '+' marker symbol.

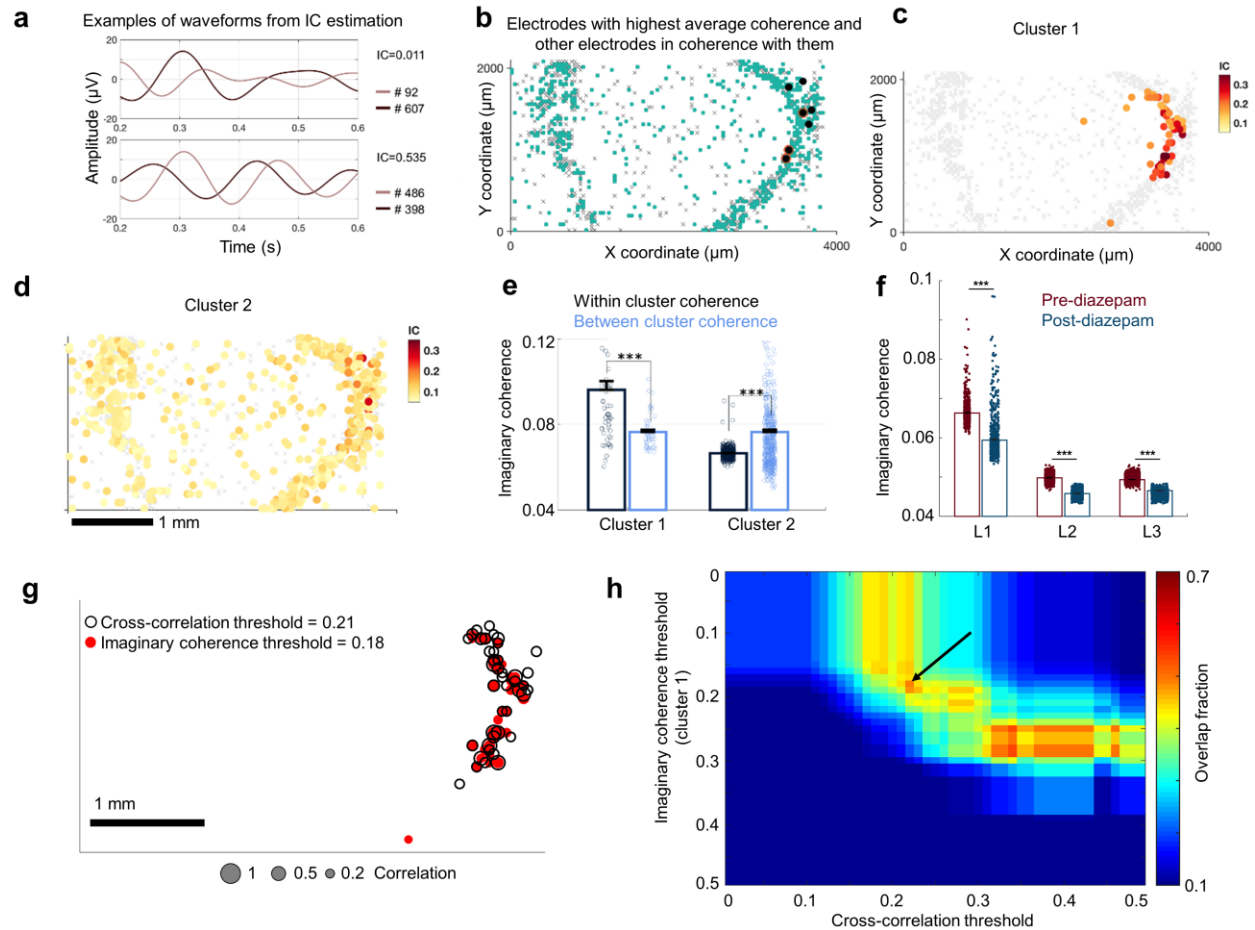


Supplementary Fig. 17. Theta amplitude within and outside of population bursts. a,b

Examples of theta frequency and multi-unit activity population averaged firing rate (5 ms average) from electrode sites measured from organoid L2 and L1 respectively. **c** The time that theta oscillations remain above the noise floor increases during population bursts. For each array (at 7 months old), the number of channels that had a correlation score of at least 0.15 with the top correlated reference ‘seed’ channel was selected. From these channels, the number of channels with at least a 10% increase in the fraction of time that the theta envelope exceeds 1.5 rms for burst periods vs non-burst periods is plotted (blue) and the number of channels with at least a 10% decrease is plotted (red). In all cases, the number of channels with at least a 10% increase is larger, indicating that there are more channels with a higher amplitude during burst periods versus non-burst periods than there are channels with a lower amplitude during burst periods versus non-burst periods for $n = 4$ organoids (organoid L4 and L6 were omitted due to low population rate activity compared to the other organoids).

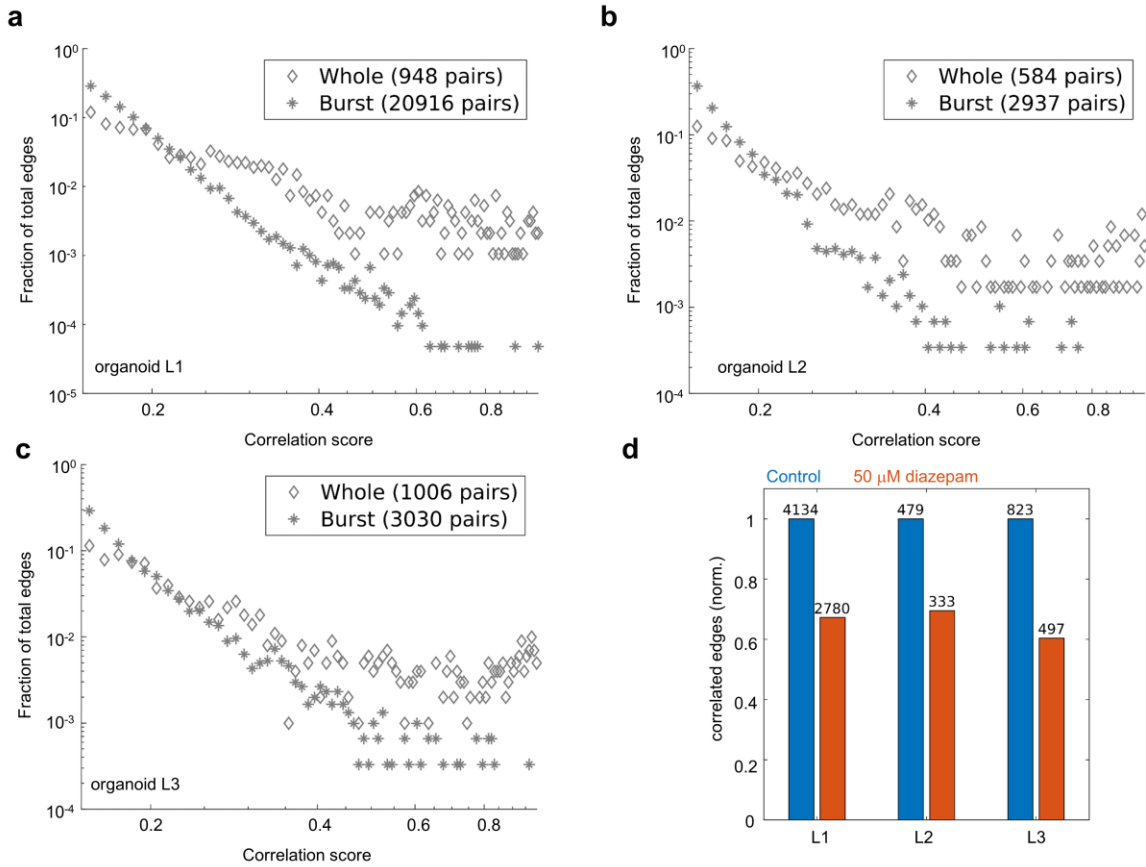


Supplementary Fig. 18. Spatiotemporal activation of theta oscillations and synchronization with neuronal population bursts. **a** Spatial snapshots of theta oscillation amplitudes are shown across the organoid L1 (8 months old) at various time points during an epoch of increased neuronal synchrony during a population burst. Positive theta amplitudes originate on the right side and spread towards the left portion of the ring-like region of activity highlighted by cross-correlation analysis shown in **Fig. 7d-f**. Each pixel represents the theta amplitude averaged over a five-by-five electrode grid, where each pixel is spaced at a distance of 35 μm . **b-h** Additional example of correlated theta activity for organoid L2 at 8 months. **b** The raw local field potential (< 500 Hz, black line) and the 4-8 Hz theta filtered band (red) (top). The phase of the theta oscillation (bottom). **c** Theta band oscillations (red) from four different recording sites and the population-averaged firing rate (black, 100 ms average). **d** Zoomed in view of highlighted gray rectangle in **c**. The solid lines indicate the relative phase offsets of theta oscillations across spatial sites of the organoid. **e** Spatial correlation map of theta oscillations. The correlation coefficient (bubble size) is shown with respect to the seed reference site (3) and the relative time-lag with respect to the reference electrode is shown in grayscale. **f** Signal averaged theta oscillations using peaks from electrode (3) as a reference. The numbers 1-4 in **d-f** all refer to the same set of electrodes. **g** Spatial map of signal averaged theta oscillation phase and amplitude relative to reference electrode number 3. Two time points are shown, one at the center of the reference channel t_0 (top) and another 60 ms later (bottom). The right hand side of the upper plot has a dominant phase of around 120-180 degrees while the left hand side has more dominant clustering of phases around 240 degrees. The bottom panel has a phase advancement of roughly 100 degrees relative to the top panel. **h** Spatial snapshot of the evolution of theta amplitudes occurring during a population burst from the same organoid identified in **b-g**.

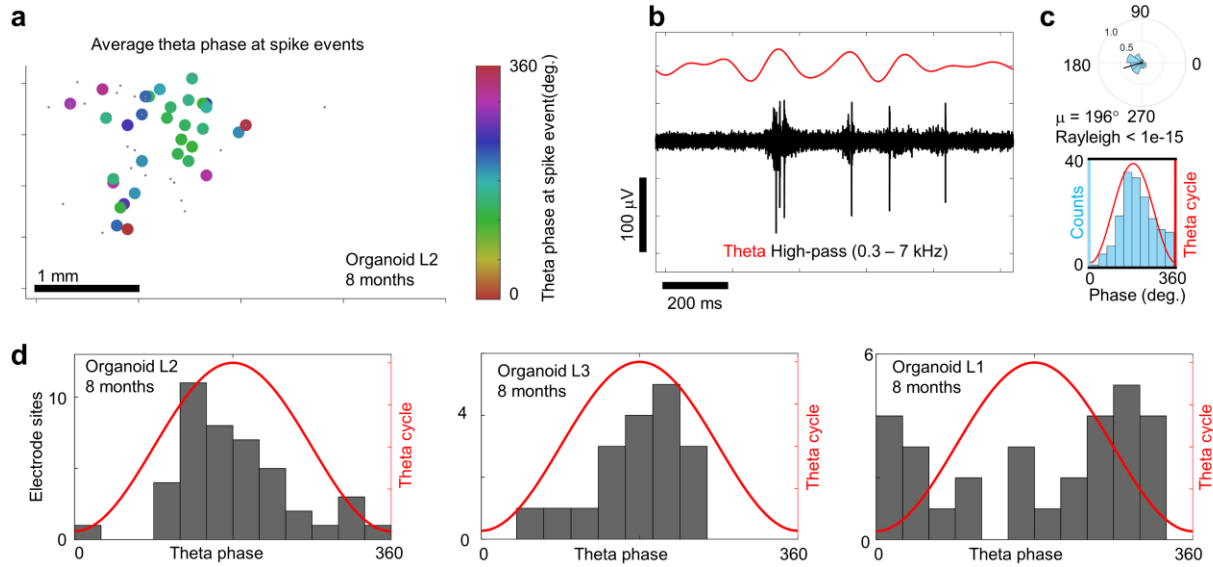


Supplementary Fig. 19. Imaginary coherence. **a** Example of theta band waveforms from two electrodes that are weakly correlation (top) and highly correlated (bottom) in the organoid (L1) using the imaginary coherence estimation. **b** Seven nodes (in black) identified as the highest coherent nodes. This cluster was identified by first calculating the node-to-node imaginary coherence and thresholding it at the top 10% of the full coherence matrix with a minimum of 200 connections. The top-seven nodes showed connections to a total of 595 nodes (shown in teal). **c-d** Among these 595 nodes, a K-means clustering procedure identified a distinct local cluster (cluster 1, **c**) as separated from the rest of the nodes which showed a lesser degree of coherence (cluster 2, **d**). **e** The local cluster showed significant higher within coherence ($n = 54$, cluster 1), depicting higher local connectivity as determined by a Wilcoxon ranked sum test ($P < 1e-4$). The rest of the nodes, labeled as cluster 2 ($n = 541$), showed relatively poor within cluster coherence. **f** The average global imaginary coherence was decreased after treatment with diazepam ($50 \mu\text{M}$) for three organoids, L1, L2 and L3 (Wilcoxon ranked sum test, $n = 1020$, $P < 1e-4$, $< 1e-4$, $< 1e-4$, for organoids L1, L2 and L3 respectively). Error bars represent the SEM for **e** and **f**. **g** Spatial plots are shown from both cross-correlation (black circles) and imaginary coherence (cluster 1 identified in **c**) analysis (red circles) for thresholds of 0.21 and 0.18, respectively. At these thresholds 44% of the electrodes identified by imaginary coherence analysis overlap with sites identified by cross-correlation analysis. **h** The fractional overlap between sites identified by imaginary coherence and cross-correlation calculations is shown as a function of correlation threshold and plotted as a heatmap. The black arrow indicates the thresholds identified in panel **g**. This analysis was performed in organoid L2 using the same thresholds specified in **g**, yielding

similar results with an overlap fraction of 51%.

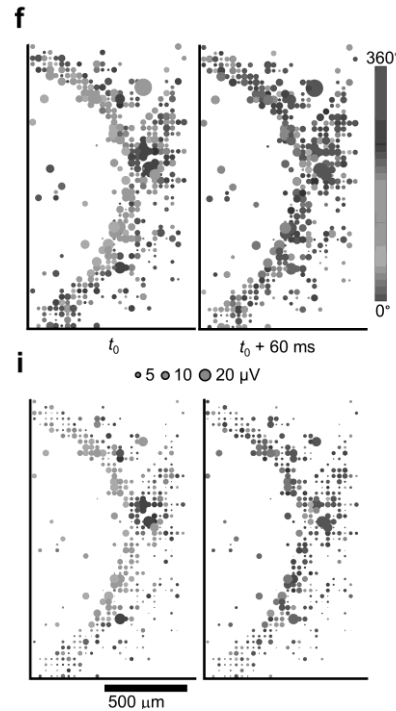


Supplementary Fig. 20. Distribution of pairwise theta correlations across organoids. **a-c** The relative fraction of theta correlation edges (between electrodes) for whole time recording and during burst epochs are shown. The number of correlated edges increases during bursts, but the relative proportion of highly correlated edges that remain outside of bursts increases. **d** The number of pairwise theta correlations between electrode sites (above 0.2) decreases for diazepam (orange) compared to control (blue).

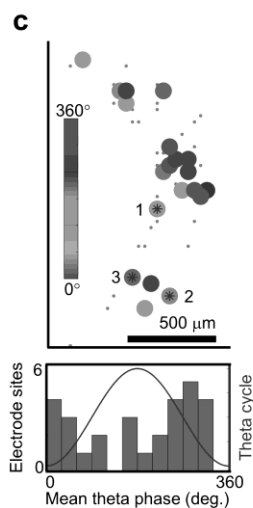


Supplementary Fig. 21. Distribution of phase-locking of spikes to theta oscillations across multiple organoids. **a** Spatial plot of phase-locked spikes to theta oscillation that satisfy the Rayleigh test for non-uniformity ($n = 43$, $P < 0.05$) for organoid L2 at 8 months. The color indicated the mean theta phase angle (μ) associated with spike events at a given electrode. The gray dots are spiking channels that do not satisfy the Rayleigh criterion ($n = 47$, $P > 0.05$). Several units share the same spatial coordinates, histograms of the single-unit mean phase-locked angles are shown in **d**. **b** Theta band (4-8 Hz) is shown in red while the spikes are shown in black in the high pass band (0.3-7 kHz) from an individual electrode from **a**. **c** Top, circular distribution of theta-spike angles measured from the electrodes in **b** over three-minute duration. Bottom, distributions of theta-spike angles shown relative to the theta cycle are visualized as a histogram plot. **d** Histogram of the mean phased-locked angle to theta for all electrode sites across the array that satisfy the Rayleigh test for non-uniformity ($n = 43$, $n = 18$, $n = 29$, $P < 0.05$) for organoid L2, L3 and L1 respectively.

Supplementary Legend 1 for Fig. 7f,i. Left panel, the inner contour of solid circles have phases around 120 degrees, while the pocket of circles on the center right consists of phases around 200-240 degrees, while the bottom left pocket consists primarily of phases around 300-360 degrees. Right panel, the phases are advanced by approximately 100 degrees. Grayscale images are shown below.



Supplementary Legend 2 for Fig. 8c. The cluster of circles directly above marker 1 ($\mu = 103$ degrees) have averages phases around 300 degrees (two circles on the bottom left of the cluster have phases around 60 and 190 degrees), while the circles neighboring marker 2 ($\mu = 189$ degrees) and marker 3 ($\mu = 16$ degrees) have phases around 200 degrees.



Supplementary Legend 3 for Fig. 9e. The circles in the upper half of the two columns have a predominate phase of around 160 degrees. The larger two dark circles in the center of the left column have phases around 190 degrees. Further down the left column, as the circles diminish in size their phase also decreases to around 160 degrees, and as the circles increase in size their phase advances to around 190 degrees. The larger circles in the center half of the right column are around 170 degrees. A grayscale image is shown below.

